

Observational constraints on the generalized α attractor model

M. Shahalam¹, Ratbay Myrzakulov², Shynaray Myrzakul³, Anzhong Wang^{1,4}

¹*Institute for Advanced Physics & Mathematics,*

Zhejiang University of Technology, Hangzhou, China

²*Eurasian International Center for Theoretical Physics,*

Department of General and Theoretical Physics,

Eurasian National University, Astana, Kazakhstan

³*Department of Theoretical and Nuclear Physics,*

Al-Farabi Kazakh National University, Al-Farabi Almaty, Kazakhstan

⁴*GCAP-CASPER, Department of Physics, Baylor University, Waco, Texas, USA*

We study the generalized α attractor model in the context of the late time cosmic acceleration. The model interpolates between the scaling freezing and thawing dark energy models. In the slow roll region, the original potential is modified whereas the modification ceases in the asymptotic region and the effective potential behaves as the quadratic one. In our setting, the field rolls slowly around the present epoch and mimics the scaling behavior in the future. We obtain observational constraints on the model parameters by using an integrated data base (SN+Hubble+BAO+CMB).

I. INTRODUCTION

The past two decades of tremendous activities in observational cosmology motivated theorists to consider various theories of gravity. This leads to a plethora of cosmological models at the theoretical ground. The observations of Type Ia supernovae by the Supernova Cosmology Project and the High-Z Supernova Search Team provided strong evidence about the currently accelerated expansion of the Universe (against the presumed decelerating expansion caused by gravity). Baryon acoustic oscillations and results from the clustering of galaxies yielded more confirmatory evidences to this acceleration. Nowadays the concept of the late time cosmic acceleration has become a fundamental ingredient for theorists in modeling the Universe. The idea of the late time cosmic acceleration is mainly attributed to the presence of some mysterious entity commonly referred to as Dark Energy [1–8]. Although there have been developed several ideas to explain the cosmic acceleration, the theory of Dark Energy is much more successful to explaining various phenomena. On the other hand, primordial inflation has taken a special status in explaining the origin of the anisotropies in the cosmic microwave background radiation (CMBR) and the formation of the large scale structure. The origin of both the early and late time inflation still represents a great theoretical puzzle which motivates theorists to invoke scalar fields to explain the two inflationary phases simultaneously. During the past three and half decades, a wide variety of inflationary models have been proposed, among which “cosmological attractors” was discovered very recently. These belong to a very broad class which incorporates the conformal attractors [9, 10], alpha attractors [11–15], and also includes scalar field cosmological models such as the Starobinsky model [16–20], the chaotic inflation in super-gravity (GL model) [21–23], Higgs inflation [24–33] and axion monodromy inflation [34–41]. All these have a mysterious fact in the context of recently released results obtained by WMAP and Planck data [42–45] that they provide the very similar cosmological predictions, although they have different origins. For conformal attractors, they predict that, for a large number of e -folds N , the spectral index and tensor-to-scalar ratio are given by $n_s = 1 - 2/N$; $r = 12/N^2$. For $N \sim 60$, these predictions are $n_s \sim 0.967$, $r \sim 0.003$, while for $N \sim 50$, $n_s \sim 0.96$, $r \sim 0.005$, which are in very good agreement with WMAP and Planck data. For α attractors, the slow roll parameters n_s and r can be written as $n_s = 1 - 2/N$, $r = 12\alpha/N^2$ for small α , and $n_s = 1 - 2/N$, $r = 12\alpha/(N(N + 3\alpha/2))$ for large α , where N is the number of e -folds between the end of inflation and horizon-crossing, and its numerical value lies in the range $50 \leq N \leq 60$. These models can be used not only for inflation but also for the late time cosmic acceleration [46–53]. In this paper, we shall study the generalized α attractor model in the context of the late time cosmic acceleration.

The paper is organized as follows. In Section II, we present the basics of the α attractor models. Section III displays the evolution equations of the scalar field in the autonomous form and addresses the issue of the cosmological attractor. In Section IV, we use the joint data to carry out observational analyses and obtain constraints on the model parameters. Our results are summarized in Section V.

II. α - MODELS

Here, we focus on the minimally coupled alpha attractors which are of more interest as they play an important role in cosmology to investigate the dark energy properties and to evaluate if these models can explain the late time cosmic acceleration. In the Einstein frame, the Lagrangian density of the alpha attractor model takes the form,

$$\mathcal{L} = \sqrt{-g} \left[\frac{1}{2} M_p^2 R - \frac{\alpha}{\left(1 - \frac{\varphi^2}{6}\right)^2} \frac{(\partial\varphi)^2}{2} - \alpha f^2 \left(\frac{\varphi}{\sqrt{6}} \right) \right] \quad (1)$$

with a real scalar field φ . Despite of the changes in the inflaton potential and an arbitrary function $f(\varphi)$, this class of models has similar striking results for the primordial scalar perturbation tilt and tensor-to-scalar ratio. For $\alpha = 1$, the Starobinsky model is recovered. We would like to note that the kinetic and potential energies have the same overall coefficient α . The kinetic term is not canonical, but can be so through a field redefinition $\phi = \sqrt{6\alpha} \tanh^{-1} \left(\frac{\varphi}{\sqrt{6}} \right)$ with $V(\phi) = \alpha f^2 \left(\tanh \left(\frac{\phi}{\sqrt{6\alpha}} \right) \right)$. We are interested in the dynamics of the scalar field and the evolution of its equation of state, and see whether it explains the late-time cosmic acceleration.

Two functional forms of f have been employed for inflation,

$$f = c \tanh \left(\frac{\phi}{\sqrt{6\alpha}} \right), \quad (2)$$

$$\text{and } f = c \frac{\tanh \left(\frac{\phi}{\sqrt{6\alpha}} \right)}{1 + \tanh \left(\frac{\phi}{\sqrt{6\alpha}} \right)} \quad (3)$$

The first one is known as the T model and the second one is the Starobinsky model ($\alpha=1$). Both models are identical at small ϕ and behave as the quadratic potential near the origin.

We consider a generalized α model given by [54]

$$f = c \frac{\tanh \left(\frac{\phi}{\sqrt{6\alpha}} \right)}{\left(1 + \tanh \left(\frac{\phi}{\sqrt{6\alpha}} \right) \right)^n} \quad (4)$$

where c is a constant, α is a parameter, and n is a number which can take the values $n = 0, 1, 2, 3, \dots$. Therefore, the potential of the generalized α model becomes

$$V(\phi) = \alpha c^2 \frac{\tanh \left(\frac{\phi}{\sqrt{6\alpha}} \right)^2}{\left(1 + \tanh \left(\frac{\phi}{\sqrt{6\alpha}} \right) \right)^{2n}} \quad (5)$$

As $\phi \rightarrow \infty$, the potential becomes constant (flatten), and as $\phi \rightarrow 0$, it behaves as a quadratic potential (see Figure 1).

III. EVOLUTION EQUATIONS AND ATTRACTORS

Caldwell and Linder [55] revealed that the scalar field models can be divided into two categories: the fast roll (freezing) and slow roll (thawing) models. A freezing model is such that, during the matter/radiation era, the field mimics the background and remains sub-dominant. Only at late times, the field exits to late time cosmic acceleration. The freezing models remain independent for a wide range of initial conditions. This class corresponds to tracking freezing model. The another sub-class of freezing models is associated with the scaling solutions [56]. In this case, the energy density of the scalar field scales with the background energy density during most of the matter era.

In contrast, the thawing models are alike to inflaton that derives the acceleration of the Universe at early epoch. In the thawing models, the scalar field is initially frozen due to a large Hubble damping and behaves as a cosmological constant with $w \approx -1$. At late times the Hubble damping decreases and the scalar field slowly thaws from the frozen state and deviates from behavior of the cosmological constant.

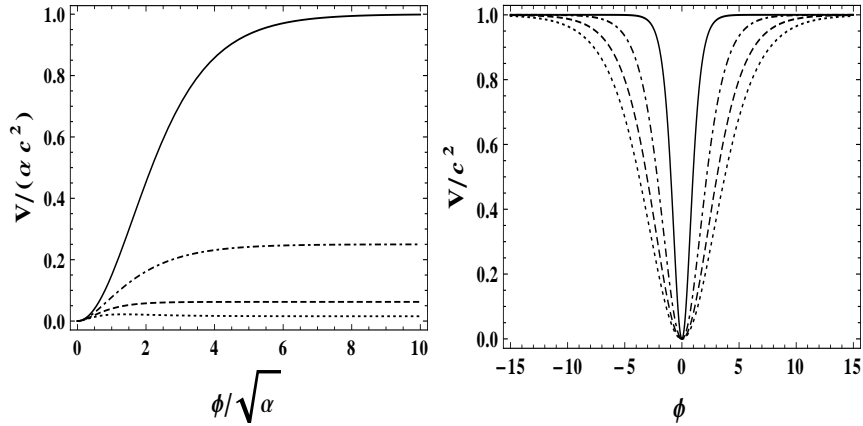


FIG. 1: In the left panel, the potential (5) of the generalized α model is plotted against $\phi/\sqrt{\alpha}$, for $n = 0, 1, 2, 3$ (from top to bottom). For large field values ($\phi \gg \sqrt{\alpha}$), the potential becomes constant and for small field values ($\phi \ll \sqrt{\alpha}$), it behaves as a quadratic potential. The right panel shows the evolution of the potential versus the field ϕ for different values of α . The dot, dashed, dot-dashed and solid lines represent the values of $\alpha = 3, 2, 1, 0.2$, respectively. The smaller α corresponds to a more narrow minimum of the potentials. This panel is plotted only for $n = 0$. In both panels, the potential and field are shown in units of c^2 and Planck, respectively.

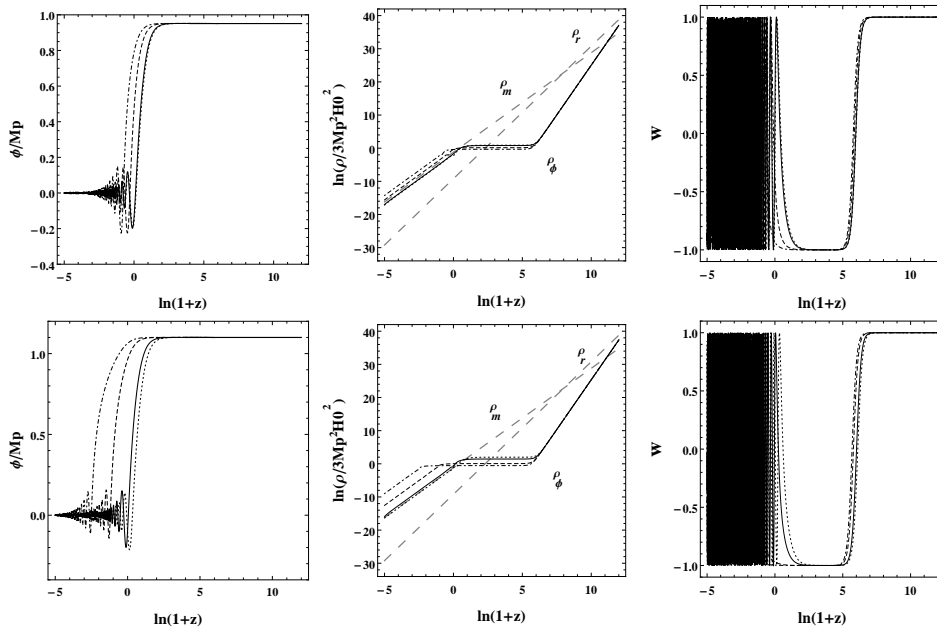


FIG. 2: The figure exhibits the evolution of the field ϕ , energy density ρ and equation of state w versus the redshift z . The dot-dashed, dashed, solid, and dotted lines correspond to the evolution of ϕ , ρ_ϕ and w for $\alpha = 0.05, 0.1, 1, 10$, respectively. The big dashed (—) lines represent the evolution of the energy densities of matter and radiation. In the upper and lower left panels, the field evolves from plateau region, as the time passes, it approaches to origin and gives rise to oscillating behavior. The upper and lower middle panels show that, initially the field energy density ρ_ϕ is sub-dominant and remains so for almost all of the period of the evolution. At late times, ρ_ϕ catches up with the energy density of the background (big dashed lines) and eventually overtakes it. Around the present epoch, ρ_ϕ lies in the thawing region as the field freezes due to a large Hubble damping, and in future it scales with the background. The upper and lower right panels show the evolution of the equation of state w . At the present epoch, it acts as a thawing, and in future as the field approaches to origin, the equation of state oscillates between $+1$ and -1 , and the system spends most of the time around $w = \pm 1$. The upper panels are plotted for $\Omega_{0m} = 0.3$, $c = 7M_p H_0$ and $n = 0$ whereas the lower panels are for $\Omega_{0m} = 0.3$, $c = 12M_p H_0$ and $n = 1$.

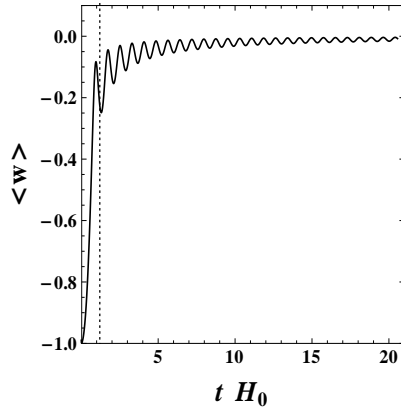


FIG. 3: The figure displays the average equation of state versus the cosmic time. In the future, the potential behaves as a quadratic potential whose average equation of state is $\langle w \rangle = 0$ at the attractor point, as shown in the figure, which is consistent with the analytical solution (8). The vertical dotted line represents the present epoch.

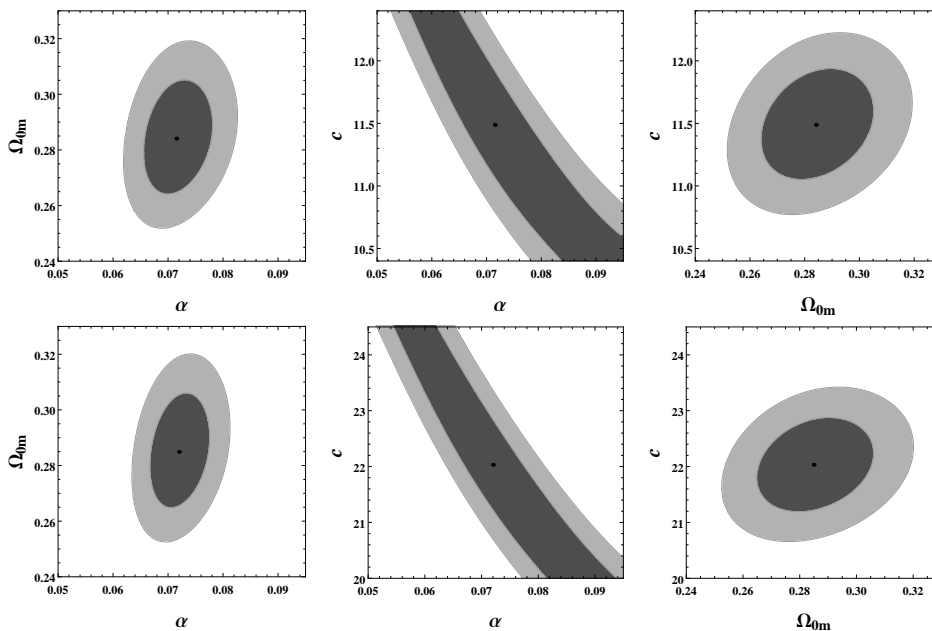


FIG. 4: Top and bottom panels show 1σ (dark shaded) and 2σ (light shaded) likelihood contours for $n = 1, 2$, respectively. We have used the joint data (SN + Hubble + BAO + CMB) to carry out the data analysis. The black dots represent the best-fitting values of the parameters.

Thawing models are much sensitive to initial conditions. Some of the models of this class have been studied in [57, 58]. The thawing, tracker and scaling models have been discussed in [59].

The α attractor models seem to combine these two classes in one way. We consider the potential given by equation (5), which has the following asymptotic form

$$V(\phi) \approx \alpha c^2 2^{-2n} \left(1 - 2(2-n)e^{-\frac{2\phi}{\sqrt{6\alpha}}} \right), \quad \phi \gg \sqrt{\alpha} \quad (6)$$

This is an uplifted exponential potential and studied as the inflationary models [21–23]. The exponential potential falls in the freezing class and approaches to a cosmological constant.

$$V(\phi) \approx \frac{c^2}{6\alpha} \phi^2, \quad \phi \ll \sqrt{\alpha} \quad (7)$$

This is the quadratic potential, falls in the thawing class and deviates from the cosmological constant. The analytical solution of the average equation of state for the power-law potential $V(\phi) \propto \phi^{2p}$ is given

by

$$\langle w \rangle = \frac{p-1}{p+1} \quad (8)$$

For the quadratic potential $p = 1$, therefore, in this case, as ϕ approaches to the origin, the time average equation of state during the oscillations is given by $\langle w \rangle = 0$.

The equations of motion are obtained by varying the Lagrangian density (1) with equation (5) have the following forms

$$\frac{\dot{a}^2(t)}{a^2(t)} = \frac{1}{3M_{pl}^2} (\rho_r + \rho_m + \rho_\phi) \quad (9)$$

$$\ddot{\phi} + 3\frac{\dot{a}}{a}\dot{\phi} + V'(\phi) = 0 \quad (10)$$

where a prime ($'$) denotes the derivative with respect to ϕ . In the following discussions we shall use the dimensionless variables

$$Y_1 = \frac{\phi}{M_p}, \quad Y_2 = \frac{\dot{\phi}}{M_p H_0}, \quad \mathcal{V} = \frac{V(Y_1)}{M_p^2 H_0^2}. \quad (11)$$

Using these new dimensionless variables, we can cast equations (9) and (10) as a system of the first-order equations

$$Y_1' = \frac{Y_2}{h(Y_1, Y_2)} \quad (12)$$

$$Y_2' = -3Y_2 - \frac{1}{h(Y_1, Y_2)} \left[\frac{d\mathcal{V}(Y_1)}{dY_1} \right] \quad (13)$$

The prime ($'$) denotes the derivative with respect to $\ln(a)$, and the function $h(Y_1, Y_2)$ is given by,

$$h(Y_1, Y_2) = \sqrt{\left[\frac{Y_2^2}{6} + \frac{\mathcal{V}(Y_1)}{3} + \Omega_{0m} e^{-3a} + \Omega_{0r} e^{-4a} \right]} \quad (14)$$

Here, Ω_{0r} and Ω_{0m} are the energy density parameters of radiation and matter, respectively at the present epoch. We solve the evolution equations (12) and (13) numerically, and the results are shown in Figures 1 - 4. Figure 1 exhibits the behavior of the potential (5) versus the scalar field ϕ , in units of c^2 and Planck, respectively. The left panel is plotted for $n = 0, 1, 2, 3$. For large field values, the potential flattens to an uplifted plateau, while at small values it looks like the quadratic potential. The right panel is plotted for $n = 0$ with various values of α . The smaller values of α correspond to a more narrow minimum of the potential.

As the field evolving from the flatten region approaches the origin, the energy density ρ_ϕ undershoots the background and begins as thawing dark energy along with thawing behavior as the field freezes due to a large Hubble damping, and it lies in the thawing region even at the present epoch. However, in the future it switches over and converts to the scaling freezing behavior (see Figure 2).

The upper and lower right panels of Figure 2 show that the field oscillates most time between $w = \pm 1$, and correspondingly the average equation of state is $\langle w \rangle = 0$ at the attractor point (see Figure 3), which is consistent with the analytical result (8) for a quadratic potential.

Figure 4 demonstrates the 1σ (dark shaded) and 2σ (light shaded) likelihood contours in the $\alpha - \Omega_{0m}$, $\alpha - c$ and $\Omega_{0m} - c$ planes with two different values of n , for the generalized α attractor model. The joint data (SN+Hubble+BAO+CMB) have been used to carry out the observational analysis. The best-fitting values of the model parameters for two distinct values of n are shown in Table I.

Our study shows that the α attractor model behaves as a ϕ^2 potential when the scalar field approaches to origin. Before reaching the oscillatory phase, it has a slow-roll regime, which provides the late-time cosmic acceleration at the present epoch. Similar results can be obtained, if we use the ϕ^2 potential rather than the α attractor. To confirm this, we consider the quadratic potential

$$V(\phi) = V_0 \left(\frac{\phi}{M_p} \right)^2 \quad (15)$$

TABLE I: The Table represents the best-fitting values of the model parameters for two values of n .

n	α	Ω_{0m}	c
1	0.0715	0.2841	11.4884
2	0.0720	0.2849	22.0320

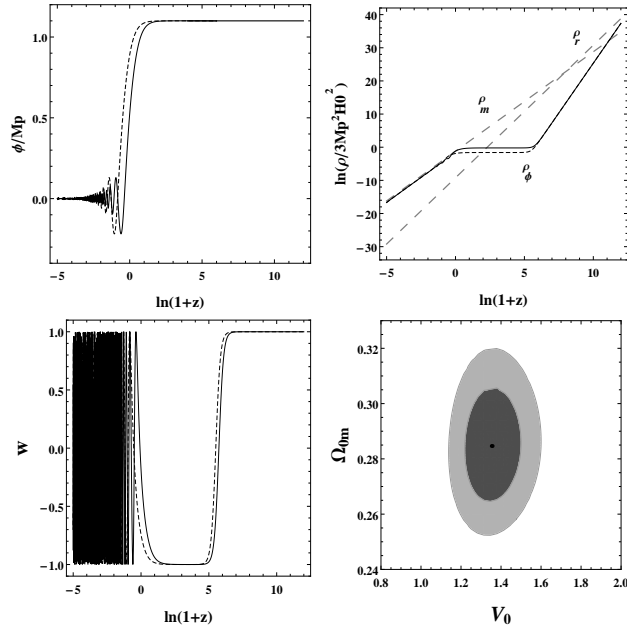


FIG. 5: This figure is plotted for the quadratic potential (15), and exhibits the evolution of the scalar field ϕ , energy density ρ and equation of state w versus the redshift z . The dashed and solid lines correspond to the evolution of ϕ , ρ_ϕ and w for two different values of $V_0 = 0.5M_p^2 H_0^2$ (dashed) and $V_0 = 2M_p^2 H_0^2$ (solid). The big dashed (—) lines represent the evolution of the energy densities of matter and radiation. The bottom right panel shows 1σ (dark shaded) and 2σ (light shaded) likelihood contours. We have used the joint data (SN+Hubble+BAO+CMB) to carry out the data analysis. The black dot designates the best-fit value of the model parameters, and found to be $V_0 = 1.3534$ and $\Omega_{0m} = 0.2846$.

We numerically evolve Eqs.(12) and (13) with (15). The results are presented in figure 5. The top and bottom left panels show the evolution of ϕ , ρ_ϕ and w versus the redshift. One can clearly see that before reaching the oscillatory phase, the field has a slow-roll regime, which gives the late-time cosmic acceleration at the current epoch. The bottom right panel exhibits the 1σ (dark shaded) and 2σ (light shaded) likelihood contours in the $V_0 - \Omega_{0m}$ plane. The best-fit values of the model parameters are found to be $V_0 = 1.3534$ and $\Omega_{0m} = 0.2846$. The best-fit values of Ω_{0m} for the quadratic potential and α model almost coincide, see Table I. Therefore, both models provide a similar late-time cosmic acceleration at the present epoch, and are consistent with current observations.

IV. DATA ANALYSIS

We employ the χ^2 analysis to constrain the model parameters. One can use the maximum likelihood method and get the total likelihood for the parameters α , Ω_{0m} and c as the product of individual likelihood for different datasets. The total likelihood function for joint data is given by

$$\mathcal{L}_{tot}(\alpha, \Omega_{0m}, c) = e^{-\frac{\chi_{tot}^2(\alpha, \Omega_{0m}, c)}{2}} \quad (16)$$

where

$$\chi_{\text{tot}}^2 = \chi_{\text{SN}}^2 + \chi_{\text{Hub}}^2 + \chi_{\text{BAO}}^2 + \chi_{\text{CMB}}^2, \quad (17)$$

is related to Type Ia supernova (SN), data of Hubble parameter, Baryon Acoustic Oscillation (BAO) and Cosmic Microwave Background (CMB) data. The best fit value of the parameters is acquired by minimizing χ_{tot}^2 with respect to α , Ω_{0m} and c . The likelihood contours in 1σ and 2σ confidence level are given as 2.3 and 6.17, respectively, in the two dimensional parametric space.

A. Type Ia Supernova

To study the Universe on a very large scale, Type Ia supernova is considered as an ideal astronomical object. They are very bright and the luminosity distance can be determined upto the redshift $z \simeq 1.4$. They have almost the same luminosity which is redshift-independent. Hence Type Ia supernova are observed as very good standard candles.

The Type Ia supernova is one of the direct probe for the cosmological expansion. We take 580 data points of latest Union2.1 compilation data [60]. In this case, one measures the apparent luminosity of the supernova explosion. The most appropriate quantity is the luminosity distance $D_L(z)$ defined as

$$D_L(z) = (1+z) \int_0^z \frac{H_0 dz'}{H(z')}. \quad (18)$$

In reality, the distance modulus $\mu(z)$ is the observed quantity which is directly related to the $D_L(z)$ as $\mu(z) = m - M = 5 \log D_L(z) + \mu_0$, where M and m are the absolute and apparent magnitudes of the Supernovae and $\mu_0 = 5 \log \left(\frac{H_0^{-1}}{\text{Mpc}} \right) + 25$ is a nuisance parameter which should be marginalized. Therefore, the corresponding χ^2 can be written as

$$\chi_{\text{SN}}^2(\mu_0, \theta) = \sum_{i=1}^{580} \frac{[\mu_{th}(z_i, \mu_0, \theta) - \mu_{obs}(z_i)]^2}{\sigma_{\mu}(z_i)^2}, \quad (19)$$

where μ_{obs} , μ_{th} and σ_{μ} represent the observed, theoretical distance modulus and uncertainty in the distance modulus respectively; θ represents any arbitrary parameter of the particular model. Eventually marginalizing μ_0 and following reference [61], we get

$$\chi_{\text{SN}}^2(\theta) = A(\theta) - \frac{B(\theta)^2}{C(\theta)}, \quad (20)$$

where,

$$A(\theta) = \sum_{i=1}^{580} \frac{[\mu_{th}(z_i, \mu_0 = 0, \theta) - \mu_{obs}(z_i)]^2}{\sigma_{\mu}(z_i)^2}, \quad (21)$$

$$B(\theta) = \sum_{i=1}^{580} \frac{\mu_{th}(z_i, \mu_0 = 0, \theta) - \mu_{obs}(z_i)}{\sigma_{\mu}(z_i)^2}, \quad (22)$$

$$C(\theta) = \sum_{i=1}^{580} \frac{1}{\sigma_{\mu}(z_i)^2}. \quad (23)$$

B. The Hubble Parameter $H(z)$

The Hubble Parameter $H(z)$ represents the expansion history of the Universe and plays a key role in joining the cosmological models and observations. Recently, Farooq and Ratra [62] compiled 28 data points for $H(z)$ in the redshift range $0.07 \leq z \leq 2.3$ which are given in Table II. To complete the data set we take $H_0 = 67.8 \pm 0.9 \text{ Km/S/Mpc}$ from Planck results [?]. We shall work with the normalized Hubble parameter, $h = H/H_0$ and apply the data to the model. In this case, the χ^2 is defined as

$$\chi_{\text{Hub}}^2(\theta) = \sum_{i=1}^{29} \frac{[h_{th}(z_i, \theta) - h_{obs}(z_i)]^2}{\sigma_h(z_i)^2}, \quad (24)$$

TABLE II: $H(z)$ measurements (in unit $[\text{km s}^{-1}\text{Mpc}^{-1}]$) and their errors [62].

z	$H(z)$ (km/s/Mpc)	σ_H (km/s/Mpc)	Reference
0.070	69	19.6	[63]
0.100	69	12	[64]
0.120	68.6	26.2	[63]
0.170	83	8	[64]
0.179	75	4	[65]
0.199	75	5	[65]
0.200	72.9	29.6	[63]
0.270	77	14	[64]
0.280	88.8	36.6	[63]
0.350	76.3	5.6	[66]
0.352	83	14	[65]
0.400	95	17	[64]
0.440	82.6	7.8	[67]
0.480	97	62	[68]
0.593	104	13	[65]
0.600	87.9	6.1	[67]
0.680	92	8	[65]
0.730	97.3	7.0	[67]
0.781	105	12	[65]
0.875	125	17	[65]
0.880	90	40	[68]
0.900	117	23	[64]
1.037	154	20	[65]
1.300	168	17	[64]
1.430	177	18	[64]
1.530	140	14	[64]
1.750	202	40	[64]
2.300	224	8	[69]

where h_{obs} and h_{th} are respectively the observed and theoretical values of the normalized Hubble parameter. Also,

$$\sigma_h = \left(\frac{\sigma_H}{H} + \frac{\sigma_{H_0}}{H_0} \right) h, \quad (25)$$

where σ_H and σ_{H_0} are the errors associated with H and H_0 respectively.

C. Baryon Acoustic Oscillation (BAO)

The early Universe composed of photons, baryons and dark matter. Photons and baryons are tightly coupled to one another through Thompson scattering, and act as a single fluid. This fluid can not collapse under gravity but it can oscillate, due to the large pressure furnished by the photons. These oscillations are known as BAO, which are the consequences of photon-baryon coupling at redshift larger than $z = 1090$.

The characteristic scale of these oscillations is governed by the sound horizon r_s at the photon decoupling epoch, given as:

$$r_s(z_*) = \frac{c}{\sqrt{3}} \int_0^{\frac{1}{1+z_*}} \frac{da}{a^2 H(a) \sqrt{1 + (3\Omega_{0b}/4\Omega_{0\gamma})a}}, \quad (26)$$

where Ω_{0b} and $\Omega_{0\gamma}$ are the present values of baryon and photon density parameter respectively, and z_* is the redshift of photon decoupling.

The BAO sound horizon scale can be used to derive the angular diameter distance D_A and the Hubble expansion rate H as a function of redshift. By measuring the subtended angle $\Delta\theta$, of the ruler of length r_s , these parameters are defined as follows:

$$\Delta\theta = \frac{r_s}{d_A(z)} \quad \text{with} \quad d_A(z) = \int_0^z \frac{dz'}{H(z')} \quad (27)$$

TABLE III: Values of $\frac{d_A(z_*)}{D_V(Z_{BAO})}$ for distinct values of z_{BAO} .

z_{BAO}	0.106	0.2	0.35	0.44	0.6	0.73
$\frac{d_A(z_*)}{D_V(Z_{BAO})}$	30.95 ± 1.46	17.55 ± 0.60	10.11 ± 0.37	8.44 ± 0.67	6.69 ± 0.33	5.45 ± 0.31

where $\Delta\theta$ is the measured angular separation of the BAO feature in the 2 point correlation function of the galaxy distribution on the sky, and

$$\Delta z = H(z)r_s, \quad (28)$$

where Δz is the measured redshift separation of the BAO feature in the 2 point correlation function along the line of sight. We work with BAO data of $d_A(z_*)/D_V(Z_{BAO})$ [70–75], where $z_* \approx 1091$ is the decoupling time, $d_A(z)$ is the co-moving angular-diameter distance and $D_V(z) = (d_A(z)^2 z / H(z))^{1/3}$ is the dilation scale. Data needed for this inspection is shown in Table III. The corresponding χ_{BAO}^2 is given as [75]:

$$\chi_{BAO}^2 = X^T C^{-1} X, \quad (29)$$

where

$$X = \begin{pmatrix} \frac{d_A(z_*)}{D_V(0.106)} - 30.95 \\ \frac{d_A(z_*)}{D_V(0.2)} - 17.55 \\ \frac{d_A(z_*)}{D_V(0.35)} - 10.11 \\ \frac{d_A(z_*)}{D_V(0.44)} - 8.44 \\ \frac{d_A(z_*)}{D_V(0.6)} - 6.69 \\ \frac{d_A(z_*)}{D_V(0.73)} - 5.45 \end{pmatrix}, \quad (30)$$

and C^{-1} is the inverse covariance matrix defined as in [75].

$$C^{-1} = \begin{pmatrix} 0.48435 & -0.101383 & -0.164945 & -0.0305703 & -0.097874 & -0.106738 \\ -0.101383 & 3.2882 & -2.45497 & -0.0787898 & -0.252254 & -0.2751 \\ -0.164945 & -2.45499 & 9.55916 & -0.128187 & -0.410404 & -0.447574 \\ -0.0305703 & -0.0787898 & -0.128187 & 2.78728 & -2.75632 & 1.16437 \\ -0.097874 & -0.252254 & -0.410404 & -2.75632 & 14.9245 & -7.32441 \\ -0.106738 & -0.2751 & -0.447574 & 1.16437 & -7.32441 & 14.5022 \end{pmatrix}. \quad (31)$$

D. Cosmic Microwave Background (CMB) distance information

The CMB measurement is sensitive to distance to the last scattering surface (decoupling epoch) via the positions of peaks and troughs of acoustic oscillations. Following the WMAP results [76], the distance information incorporates the “shift parameter” R , “acoustic scale” l_A and the redshift of last scattering surface z_{ls} , where R and l_A are the ratio of angular diameter distance to the last scattering surface over the Hubble horizon and the sound horizon at diameter of the last scattering, and are given by

$$R = H_0 \sqrt{\Omega_{0m}} \chi(z_{ls}), \quad (32)$$

$$l_A = \frac{\pi \chi(z_{ls})}{\chi_s(z_{ls})}, \quad (33)$$

where $\chi(z_{ls})$ is the co-moving distance to z_{ls} and $\chi_s(z_{ls})$ is the co-moving sound horizon at z_{ls} . The shift parameter R can also be computed theoretically using the formula

$$R = H_0 \sqrt{\Omega_{0m}} \int_0^{z_{ls}} \frac{dz'}{H(z')}. \quad (34)$$

From equation (34), we observe that R is related to the matter density as well as the expansion history of the Universe until the redshift of the surface of the last scattering, z_{ls} , which is computed through the fitting function [77]:

$$z_{ls} = 1048 [1 + 0.00124(\Omega_b h^2)^{-0.738}] [1 + g_1(\Omega_{0m} h^2)^{g_2}], \quad (35)$$

where g_1 and g_2 are defined as

$$g_1 = \frac{0.0783(\Omega_b h^2)^{-0.238}}{1 + 39.5(\Omega_b h^2)^{0.763}}, \quad (36)$$

$$g_2 = \frac{0.56}{1 + 21.1(\Omega_b h^2)^{1.81}}. \quad (37)$$

The corresponding χ^2 can be written as

$$\chi^2(\theta) = \frac{(R(\theta) - R_0)^2}{\sigma^2}, \quad (38)$$

where $R(\theta)$ depends on the model parameter θ and $R_0 = 1.725 \pm 0.018$ [76].

V. CONCLUSION

In this paper, we have investigated the generalized α attractor model that leads to the cosmological attractor behavior and can interpolate between the thawing and scaling freezing models. At the present epoch, it behaves as a thawing model whereas in the future it possesses scaling freezing behavior. In Figure 2, the dynamics of the scalar field and energy density ρ_ϕ are shown for $\alpha = 0.05, 0.1, 1, 10$. The evolution of ρ_ϕ starts off as a thawing dark energy along with thawing behavior, and even at the present epoch it lies in the thawing region. But in the future it switches over and turns to the scaling regime, which is cosmological attractor. For small values of the scalar field ϕ , the generalized α attractor model mimics the power law behavior $V(\phi) \sim \phi^2$ and produces oscillations of ϕ near the origin which are reflected in the behavior of the equation of state w (see Figure 2), and correspondingly the average equation of state parameter is $\langle w \rangle = 0$ (see Figure 3). In our setting, the scalar field remains in the slow roll regime but mimics the scaling behavior in the future. We considered two cases $n = 1, 2$, and used the joint data (SN+Hubble+BAO+CMB) to obtain the observational constraints on the model parameters. The best-fitting values of the model parameters for $n = 1, 2$ are $\alpha = 0.0715$, $\Omega_{0m} = 0.2841$ and $c = 11.4884$, and $\alpha = 0.0720$, $\Omega_{0m} = 0.2849$ and $c = 22.0320$, respectively.

We also considered the quadratic potential in order to compare with the results obtained from the α model. Figure 5 showed the evolution of ϕ , ρ_ϕ and w versus the redshift, and the 1σ (dark shaded) and 2σ (light shaded) likelihood contours in the $V_0 - \Omega_{0m}$ plane. The best-fit values of the model parameters are found to be $V_0 = 1.3534$ and $\Omega_{0m} = 0.2846$. The best-fit values of Ω_{0m} for both models are almost the same. Hence, in view of the current observations, both models are viable, and provide the late-time cosmic acceleration at the present epoch.

Acknowledgements

M.S. thanks M. Sami for making useful comments and suggestions. He is also thankful to M. Sajjad Athar for his constant encouragement throughout the work. A.W. is supported in part by NNSFC No.11375153 and No. 11675145, China.

-
- [1] E. J. Copeland, M. Sami, S. Tsujikawa, *Int. J. Mod. Phys. D* **15** (2006) 1753.
 - [2] V. Sahni, A. A. Starobinsky, *Int. J. Mod. Phys. D* **9** (2000) 373.
 - [3] M. Sami, *New Adv. Phys.* **10** (2016) 77-105.
 - [4] M. Sami, R. Myrzakulov, *Int. J. Mod. Phys. D* **25** (2016) 1630031.
 - [5] M. Sami, *Curr. Sci.* **97** (2009) 887.
 - [6] M Sami, arXiv:0901.0756v1.
 - [7] Md. Wali Hossain *et al.*, *Int. J. Mod. Phys. D* **24** (2015) 1530014.
 - [8] M. Sami, N. Dadhich, *TSPU Vestnik* 44N7 (2004) 25-36.

- [9] R. Kallosh and A. Linde, *JCAP* **07** (2013) 002.
- [10] R. Kallosh and A. Linde, *JCAP* **12** (2013) 006.
- [11] D. I. Kaiser and E. I. Sfakianakis, *Phys. Rev. Lett.* **112** (2014) 011302.
- [12] S. Ferrara, R. Kallosh, A. Linde and M. Porrati, *Phys. Rev. D* **88** (2013) 085038.
- [13] R. Kallosh, A. Linde and D. Roest, *JHEP* **11** (2013) 198.
- [14] R. Kallosh, A. Linde and D. Roest, *JHEP* **08** (2014) 052.
- [15] T. Miranda, J. C. Fabris and O. F. Piattella, *JCAP* **09** (2017) 041.
- [16] A. A. Starobinsky, *Phys. Lett. B* **91** (1980) 99.
- [17] V. F. Mukhanov and G. V. Chibisov, *JETP Lett.* **33** (1981) 532.
- [18] A. A. Starobinsky, *Sov. Astron. Lett.* **9** (1983) 302.
- [19] B. Whitt, *Phys. Lett. B* **145** (1984) 176.
- [20] L. A. Kofman, A. D. Linde and A. A. Starobinsky, *Phys. Lett. B* **157** (1985) 361.
- [21] A. S. Goncharov and A. D. Linde, *Sov. Phys. JETP* **59** (1984) 930.
- [22] A. B. Goncharov and A. D. Linde, *Phys. Lett. B* **139** (1984) 27.
- [23] A. Linde, *JCAP* **02** (2015) 030.
- [24] D. S. Salopek, J. R. Bond and J. M. Bardeen, *Phys. Rev. D* **40** (1989) 1753.
- [25] F. L. Bezrukov and M. Shaposhnikov, *Phys. Lett. B* **659** (2008) 703.
- [26] R. Fakir and W. G. Unruh, *Phys. Rev. D* **41** (1990) 1783.
- [27] D. I. Kaiser, *Phys. Rev. D* **52** (1995) 4295.
- [28] J. L. Cervantes-Cota and H. Dehnen, *Nucl. Phys. B* **442** (1995) 391.
- [29] E. Komatsu and T. Futamase, *Phys. Rev. D* **59** (1999) 064029.
- [30] S. Ferrara, R. Kallosh, A. Linde, A. Marrani and A. Van Proeyen, *Phys. Rev. D* **83** (2011) 025008.
- [31] S. Ferrara, R. Kallosh, A. Linde, A. Marrani and A. Van Proeyen, *Phys. Rev. D* **82** (2010) 045003.
- [32] A. Linde, M. Noorbala and A. Westphal, *JCAP* **03** (2011) 013.
- [33] R. Kallosh and A. Linde, *JCAP* **06** (2013) 027.
- [34] E. Silverstein and A. Westphal, *Phys. Rev. D* **78** (2008) 106003.
- [35] L. McAllister, E. Silverstein and A. Westphal, *Phys. Rev. D* **82** (2010) 046003.
- [36] J. P. Conlon, *JCAP* **01** (2012) 033.
- [37] R. Flauger, L. McAllister, E. Pajer, A. Westphal and G. Xu, *JCAP* **06** (2010) 009.
- [38] S. Hannestad, T. Haugbolle, P. R. Jarnhus and M. S. Sloth, *JCAP* **06** (2010) 001.
- [39] R. Flauger, L. McAllister, E. Silverstein, A. Westphal, arXiv:1412.1814.
- [40] T.C. Bachlechner, C. Long, and L. McAllister, *JHEP* **01** (2016) 091.
- [41] J. Brown, W. Cottrell, G. Shiu, and P. Soler, arXiv:1607.00037.
- [42] Planck Collab. (P. A. R. Ade *et al.*, *Astron. Astrophys.* **571** (2014) A22.
- [43] Planck Collab. (P. A. R. Ade *et al.*, *A & A* **571** (2014) A16.
- [44] Planck Collab. (P. A. R. Ade *et al.*, arXiv:1502.02114 [astro-ph.CO].
- [45] Planck Collab. (P. A. R. Ade *et al.*, *A & A* **594** (2016) A13.
- [46] S. Ferrara, R. Kallosh and A. Linde, *JHEP* **10** (2014) 143.
- [47] I. Antoniadis, E. Dudas, S. Ferrara and A. Sagnotti, *Phys. Lett. B* **733** (2014) 32.
- [48] R. Kallosh and A. Linde, *JCAP* **01** (2015) 025.
- [49] G. Dall'Agata and F. Zwirner, *JHEP* **12** (2014) 172.
- [50] R. Kallosh, A. Linde and M. Scalisi, *JHEP* **03** (2015) 111.
- [51] A. B. Lahanas and K. Tamvakis, *Phys. Rev. D* **91** (2015) 085001.
- [52] R. Kallosh and A. Linde, *Phys. Rev. D* **91** (2015) 083528.
- [53] J. J. M. Carrasco, R. Kallosh and A. Linde, *JHEP* **10** (2015) 147.
- [54] E. V. Linder, *Phys. Rev. D* **91** (2015) 123012.
- [55] R. R. Caldwell and E. V. Linder, *Phys. Rev. Lett.* **95** (2005) 141301.
- [56] E. J. Copeland, A. R. Liddle, and D. Wands, *Phys. Rev. D* **57** (1998) 4686.
- [57] M. Shahalam, S. Sami, A. Agarwal, *Mon. Not. R. Astron. Soc.* **448** (2015) 2948–2959.
- [58] R. Myrzakulov and M. Shahalam, *Gen. Rel. Grav.* **47** (2015) 81.
- [59] T. Chiba, A. D. Felice and S. Tsujikawa, *Phys. Rev. D* **87** (2013) 083505.
- [60] N. Suzuki, D. Rubin, C. Lidman, G. Aldering, R. Amanullah, K. Barbary, L. F. Barrientos and J. Botyanszki *et al.*, *Astrophys. J.* **746** (2012) 85.
- [61] R. Lazkoz, S. Nesseris, L. Perivolaropoulos, *J. Cosmol. Astropart. Phys.* bf11 (2005) 010.
- [62] O. Farooq and B. Ratra, *Astrophys. J.* **766** (2013) L7.
- [63] C. Zhang, H. Zhang, S. Yuan, T. -J. Zhang and Y. -C. Sun, arXiv:1207.4541 [astro-ph.CO].
- [64] J. Simon, L. Verde and R. Jimenez, *Phys. Rev. D* **71** (2005) 123001.
- [65] M. Moresco, L. Verde, L. Pozzetti, R. Jimenez and A. Cimatti, *JCAP* **07** (2012) 053.
- [66] C. -H. Chuang and Y. Wang, arXiv:1209.0210 [astro-ph.CO].
- [67] C. Blake, S. Brough, M. Colless, C. Contreras, W. Couch, S. Croom, D. Croton and T. Davis *et al.*, *Mon. Not. Roy. Astron. Soc.* **425** (2012) 405.
- [68] D. Stern, R. Jimenez, L. Verde, M. Kamionkowski and S. A. Stanford, *JCAP* **1002** (2010) 008.
- [69] N. G. Busca, T. Delubac, J. Rich, S. Bailey, A. Font-Ribera, D. Kirkby, J. M. Le Goff and M. M. Pieri *et al.*, *Astron. Astrophys.* **552** (2013) A96.
- [70] C. Blake, E. Kazin, F. Beutler, T. Davis, D. Parkinson, S. Brough, M. Colless and C. Contreras *et al.*, *Mon. Not. Roy. Astron. Soc.* **418** (2011) 1707.

- [71] SDSS Collab. (W. J. Percival *et al.*), *Mon. Not. Roy. Astron. Soc.* **401** (2010) 2148.
- [72] F. Beutler, C. Blake, M. Colless, D. H. Jones, L. Staveley-Smith, L. Campbell, Q. Parker and W. Saunders *et al.*, *Mon. Not. Roy. Astron. Soc.* **416** (2011) 3017.
- [73] N. Jarosik, C. L. Bennett, J. Dunkley, B. Gold, M. R. Greason, M. Halpern, R. S. Hill and G. Hinshaw *et al.*, *Astrophys. J. Suppl.* **192** (2011) 14.
- [74] D. J. Eisenstein *et al.* [SDSS Collaboration], *Astrophys. J.* **633** (2005) 560.
- [75] R. Giotri, M. V. d. Santos, I. Waga, R. R. R. Reis, M. O. Calvao and B. L. Lago, *JCAP* **1203** (2012) 027.
- [76] E. Komatsu *et al.*, *ApJS* **192** (2011) 18.
- [77] W. Hu and N. Sugiyama, *Astrophys. J.* **471** (1996) 30.